

An Unusual Twin-His Arrangement in the Pore of Ammonia Channels Is Essential for Substrate Conductance^{*[S]}

Received for publication, August 31, 2006 Published, JBC Papers in Press, October 12, 2006, DOI 10.1074/jbc.M608325200

Arnaud Javelle^{†§}, Domenico Lupo[§], Lei Zheng[§], Xiao-Dan Li[§], Fritz K. Winkler^{§1}, and Mike Merrick^{‡2}

From the [‡]Department of Molecular Microbiology, John Innes Centre, Colney Lane, Norwich, Norfolk, NR4 7UH, United Kingdom and the [§]Biomolecular Research, Paul Scherrer Institut, CH-5232 Villigen, Switzerland

Amt proteins constitute a class of ubiquitous integral membrane proteins that mediate movement of ammonium across cell membranes. They are homotrimers, in which each subunit contains a narrow pore through which substrate transport occurs. Two conserved histidine residues in the pore have been proposed to be necessary for ammonia conductance. By analyzing 14 engineered polar and non-polar variants of these histidines, in *Escherichia coli* AmtB, we show that both histidines are absolutely required for optimum substrate conductance. Crystal structures of variants confirm that substitution of the histidine residues does not affect AmtB structure. In a subgroup of Amt proteins, found only in fungi, one of the histidines is replaced by glutamate. The equivalent substitution in *E. coli* AmtB is partially active, and the structure of this variant suggests that the glutamate side chain can make similar interactions to those made by histidine.

Ammonium is the preferred nitrogen source for many organisms, and its transport across cellular membranes is a fundamental biological process. (In this report, we use the term ammonium to refer to both the protonated (NH₄⁺) and the unprotonated (NH₃) forms and ammonia to refer specifically to NH₃.) Ammonium transport is mediated by a family of ubiquitous membrane proteins (designated Amt), found in bacteria, archaea, fungi, and plants, whose homologues in animals are the Rhesus (Rh)³ proteins (1, 2). Evidence is accumulating that Rh proteins also facilitate the transport of ammonium (3, 4), but the mechanism of action of both the Amt and Rh proteins is not yet understood.

Escherichia coli encodes a single Amt protein, AmtB, which is a stable trimer in the cytoplasmic membrane and retains this structure when purified and reconstituted in the presence of lipids (5, 6). X-ray crystallographic structures of *E. coli* AmtB and of the orthologue *Archaeoglobus fulgidus* Amt-1 have

revealed a narrow channel within each monomer (7–9). At its periplasmic end, a binding site for NH₄⁺ has been identified, but entry from this site into the channel appears sterically hindered by the side chains of two conserved phenylalanines (Phe-107 and Phe-215 in AmtB). The structure analysis of *E. coli* AmtB (7, 8) led to the conclusion that the protein is a channel that conducts uncharged NH₃. Stopped-flow experiments with purified AmtB reconstituted into proteoliposomes (7) and *in vivo* functional characterization of *E. coli* AmtB are consistent with this view (10). A variety of studies on Rh proteins also support an ammonia channel model (11–13).

Almost all Amt/Rh proteins contain two conserved histidines, which in AmtB are located within transmembrane helices M5 (His-168) and M10 (His-318) such that their side chains protrude into the channel (14). They are related by the 2-fold quasi-symmetry of AmtB, and their adjacent imidazole rings are arranged such that an unusual lateral hydrogen bond is formed between their two δ1 nitrogens. It has been proposed that these histidines might have a role in the deprotonation of ammonium ions before they traverse the channel as uncharged NH₃ (4, 7, 8). Alternatively, it has been suggested that deprotonation of NH₄⁺ occurs at the periplasmic binding site through some general base present in the periplasm (4) or, based on molecular dynamics simulations, through a highly conserved Asp residue (Asp-160 in *E. coli* AmtB) (15). In a number of fungal Amt proteins, a Glu residue replaces the His-168 orthologue, and these proteins can also facilitate ammonium transport (16–18).

Site-directed mutants offer the possibility of testing some of these predictions. In this study, we report the first such analysis and confirm that the unusual twin-His structure in the pore of AmtB is essential for optimum substrate conductance.

EXPERIMENTAL PROCEDURES

Strains, Plasmids, and Culture Conditions—Strains and plasmids are listed in Table 1. Mutagenesis primers are listed in Supplemental Table SI. Growth of *E. coli* was as described previously (10). To construct pJT6E (the template for all PCR experiments), the PvuI-BamHI fragment from pGC2 was cloned into PvuI-BamHI-cut pJT6. pAJ2011 and pAJ2012 were constructed using the QuikChangeTM mutagenesis kit (Stratagene). pAJ2014, pAJ2015, pAJ2017, and pAJ2036-pAJ2045 were constructed according to a published method (19). The vector for pAJ2045 was pET22b.

Fractionation, AmtB Purification, and Western Blotting—*E. coli* AmtB was purified as described (5). Cell fractionation and Western blotting were as described (20) using polyclonal

* This work was supported by a grant from the BBSRC (to A. J. and M. M.). The costs of publication of this article were defrayed in part by the payment of page charges. This article must therefore be hereby marked "advertisement" in accordance with 18 U.S.C. Section 1734 solely to indicate this fact.

[S] The on-line version of this article (available at <http://www.jbc.org>) contains a supplemental table.

The atomic coordinates and structure factors (codes 2NMR, 2NOP, 2NPC, 2NOW, 2NPD, 2NPE, 2NPG, 2NPJ, and 2NPK) have been deposited in the Protein Data Bank, Research Collaboratory for Structural Bioinformatics, Rutgers University, New Brunswick, NJ (<http://www.rcsb.org/>).

¹ Supported by the Swiss National Science Foundation within the framework of the NCCR Structural Biology program.

² To whom correspondence should be addressed. Tel.: 44-1603-450749; Fax: 44-1603-450778; E-mail: mike.merrick@bbsrc.ac.uk.

³ The abbreviations used are: Rh, Rhesus; GS, glutamine synthetase; r.m.s., root mean square.

anti-rabbit antibodies raised against *E. coli* proteins, AmtB (21), GS (W. van Heeswijk), or GlnK (J. Thornton).

Protein Quantification—For each AmtB variant, serial dilutions of whole-cell extracts of strain GT1000 (Δ glnK Δ amtB) expressing a mutant *amtB* allele were subject to Western blotting using anti-AmtB antibodies. On each gel, 20, 14, 10, and 6 ng of pure AmtB were loaded for quantification. X-ray films were scanned and analyzed using GeneTools software (Syngene).

[¹⁴C]Methylammonium Transport Assays—Methylamine accumulation (AmtB activity) and methylglutamine accumulation (glutamine synthetase activity) were determined as described (10).

TABLE 1
E. coli strain and plasmids used in this study

Strain/plasmid	Genotype	Relevant phenotype	Reference/ source
Strain GT1000	<i>rbs lacZ::IS gyrA hutC^K</i> Δ glnK Δ amtB	Δ AmtB	20
Plasmids			
pAJ2011	<i>glnK amtB19</i>	AmtBH318A	This work
pAJ2012	<i>glnK amtB17</i>	AmtBH168E	This work
pAJ2014	<i>glnK amtB16</i>	AmtBH168A	This work
pAJ2015	<i>glnK amtB18</i>	AmtBH168F	This work
pAJ2017	<i>glnK amtB20</i>	AmtBH318F	This work
pAJ2036	<i>glnK amtB21</i>	AmtBH168Q	This work
pAJ2037	<i>glnK amtB22</i>	AmtBH168N	This work
pAJ2038	<i>glnK amtB23</i>	AmtBH168K	This work
pAJ2039	<i>glnK amtB24</i>	AmtBH168D	This work
pAJ2040	<i>glnK amtB25</i>	AmtBH168T	This work
pAJ2041	<i>glnK amtB26</i>	AmtBH318E	This work
pAJ2042	<i>glnK amtB27</i>	AmtBH318T	This work
pAJ2043	<i>glnK amtB28</i>	AmtBH168E/H318E	This work
pAJ2044	<i>glnK amtB29</i>	AmtBH168T/H318T	This work
pAJ2045	<i>glnKamtB30</i>	AmtBH168A/H318A	This work
pJT6E	<i>glnKamtB15</i>	AmtB	This work
pJT6	<i>glnKamtB9</i>	AmtB	21
pGC2	<i>glnKamtB1</i>	AmtB	21

TABLE 2
Data collection and refinement statistics

	Wild-type	Wild-type	H168A	H168E	H168F	H318A	H318F	H318F	H168A/H318A
Data collection									
PDB code	2NMR	2NOP	2NPC	2NOW	2NPD	2NPE	2NPG	2NPJ	2NPK
Crystallization	<i>a,b</i>	<i>b,c</i>	<i>b,c</i>	<i>a,b</i>	<i>b,c</i>	<i>a,d</i>	<i>a,b</i>	<i>b,c</i>	<i>b,c</i>
Cell dimensions	109.79; 84.41	109.88; 84.17	109.19; 84.56	110.07; 84.62	109.31; 84.41	109.25; 84.39	109.59; 84.47	110.51; 84.18	109.92; 84.20
<i>a, c</i> (in Å), all P6 ₃									
Wavelength (Å)	0.98007	0.901031	0.96115	0.97625	0.98017	0.94998	0.99778	0.901031	0.97934
Resolution (Å)	50.0-2.1	50.0-2.0	50.0-2.1	50.0-2.2	50.0-2.1	50.0-2.1	50.0-2.0	50.0-2.0	50.0-2.0
Completeness (%)	99.5	93.1	89.5	99.0	99.2	99.1	99.9	93.4	99.8
R_{sym} (%) ^{e,f}	7.2 (69.9)	6.8 (42.8)	7.9 (82.1)	8.2 (75.9)	6.9 (56.4)	11.9 (75.8)	9.7 (84.2)	9.3 (56.4)	8.6 (75.0)
I/σ	13.5 (3.1)	21.6 (5.6)	13.3 (2.5)	19.9 (3.2)	14.9 (3.6)	9.9 (2.5)	15.3 (2.7)	20.4 (6.2)	18.2 (3.1)
Reflections (total/unique)	127,509	398,193	189,190	243,915	187,926	167,452	294,329	420,118	427,325
	33,648	36,385	30,006	29,401	33,268	33,189	38,954	36,960	39,048
Refinement statistics									
R_{cryst} (%) ^g	16.4 (23)	16.0 (20)	17.0 (29)	16.1 (24)	17.2 (26)	21.1 (35)	17.9 (30)	15.7 (16)	16.5 (26)
R_{free} (%) ^g	19.5 (25)	17.8 (23)	22.3 (37)	19.5 (28)	19.8 (32)	25.3 (41)	21.2 (34)	16.8 (18)	19.0 (29)
r.m.s. deviation bond lengths (Å)	0.012	0.012	0.013	0.012	0.013	0.019	0.013	0.011	0.011
r.m.s. deviation bond angles (°)	1.4	1.3	1.3	1.4	1.5	1.9	1.5	1.2	1.4
C_{α} r.m.s. deviation (Å) ^h	0.47	0.37	0.40	0.37	0.43	0.42	0.42	0.37	0.42
Difference peak at S1 (σ)	6.5	14.4	10.2	6.7	12.5	4.9	8.9	14.4	13.3
Difference peak at S2 (σ)	2.9	<2	2.7	10.8	<2	<2	<2	<2	<2
Difference peak at S3 (σ)	4.3	4.3	5.8	5.5	<2	<2	<2	<2	<2
Difference peak at S4 (σ)	4.5	6.9	<2	5.7	<2	<2	<2	<2	<2

^a Protein stock solution: 10 mM Tris/HCl pH = 7.6, 100 mM NaCl 10% glycerol, 4 mM lauryldimethylamine oxide.

^b Reservoir solution: 0.1 M NaOAc pH = 4.6, 0.2 M (NH₄)₂SO₄ and 25–30% polyethylene glycol 400 or 550.

^c Protein stock solution: 25 mM Na-phosphate pH = 7.8, 500 mM NaCl, 10% glycerol, 4 mM lauryldimethylamine oxide, 300 mM imidazole.

^d Reservoir solution: 0.1 M NaOAc pH = 4.6, 0.2 M MgSO₄ and 25–30% polyethylene glycol 400 or 550.

^e $R_{\text{sym}} = \sum_{hkl} \sum_i |I(hkl; i) - \langle I(hkl) \rangle| / \sum_{hkl} \sum_i I(hkl; i)$.

^f Values in parentheses are for the outmost resolution shells. Their width is 0.1 Å for the data collection statistics and 0.04–0.06 Å for the refinement statistics.

^g R_{cryst} ; $R_{\text{free}} = \sum_{hkl} |F_{\text{obs}}(hkl) - F_{\text{calc}}(hkl)| / \sum_{hkl} F_{\text{obs}}(hkl)$ whereby the summation runs over the working set and test set reflections, respectively.

^h r.m.s. deviation of superimposed C_{α} structures using 357 C_{α} atoms and 1XQF (8) as reference structure.

Production, Crystallization, and Structure Analysis of Wild-type and Mutant AmtB—Cloning, expression, purification, and crystallization methods were essentially as described (8) except that we used strain C43(DE3) throughout (22). M9 medium was used for wild-type AmtB and the H318F mutant, and the auto-induction medium (23) was used in all other cases. The mutant AmtB proteins (except for H168E and H318F) were extracted from a low spin pellet (40,000 \times g) obtained after removing unbroken cells at 10,000 \times g. Affinity chromatography was performed using either Ni²⁺- or Co²⁺-loaded fast flow Sepharose beads (Amersham Biosciences). A one-step affinity purification was used in most cases, and the eluted AmtB-containing fractions, after concentration, were directly used to set up crystallization trials. Crystals were obtained by mixing 1–2 μ l of concentrated protein (10–20 mg/ml) with an equal volume of reservoir buffer in sitting drops at 20 °C (Table 2). Crystals grown after one-step purification had imidazole (about 150 mM) and higher salt (250 rather than 50 mM) in their mother liquor when compared with those grown after additional gel filtration (8). The pH in the crystallization setups containing imidazole was 6.0 and 4.6 in the others.

Crystals were mounted on cryoloops, and data collection was performed at 100 K using a marCCD detector and a rotating angle of 0.5° per image at the protein beamline X06SA or X10SA at the Swiss Light Source of the Paul Scherrer Institut in Villigen. Data sets were processed with the XDS program (24). A standardized refinement protocol was used throughout. As a starting model, we used the refined native structure 1XQF structure (8) in which His-168 and His-318 were converted to Gly and all water molecules at and in the pore, as well as those with high *B*-factors, were removed. Using Refmac (25), an initial rigid body refinement (10 cycles with data to 3 Å resolution) was followed by a round of translation/

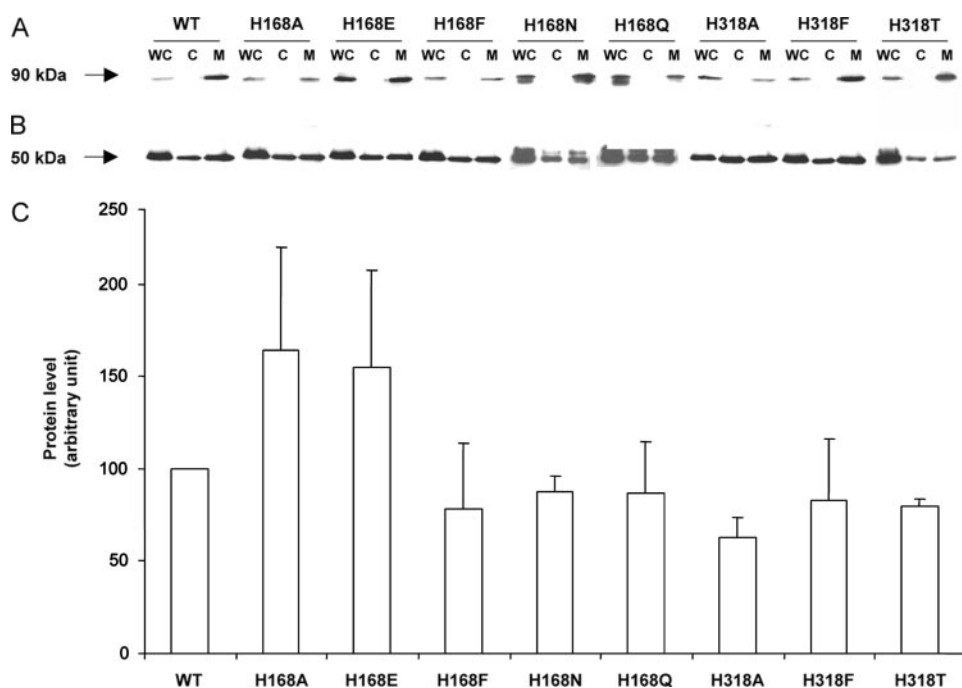


FIGURE 1. AmtB variant expression *in vivo*. Extracts from GT1000 (Δ *glnK* Δ *amtB*) expressing plasmid-encoded AmtB were used. *A*, Western blots using an anti-AmtB antibody, after SDS-PAGE of whole-cell extracts (WC), cytoplasmic (C), and membrane (M) fractions. WT, wild type. *B*, as in *A* but using anti-GS antibody. *C*, AmtB quantification. Data are from analyses using two independent batches of AmtB, four independent protein extractions for each variant, and nine different dilutions of WC.

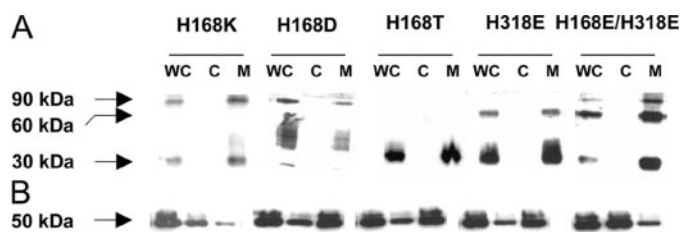


FIGURE 2. AmtB variant expression *in vivo*. Extracts from GT1000 (Δ *glnK* Δ *amtB*) expressing plasmid-encoded AmtB were used. *A*, Western blots using an anti-AmtB antibody, after SDS-PAGE of whole-cell extracts (WC), cytoplasmic (C), and membrane (M) fractions. WT, wild type. *B*, as in *A* but using anti-GS antibody.

libration/screw and restrained refinement (10 cycles with data to the maximum resolution, Table 2). After inserting the proper residues at positions 168 and 318, another 30 cycles of restrained refinement were carried out using the previously determined translation/libration/screw parameters and data between 15 Å and the maximum resolution. In this final refinement, simple scaling was used (as opposed to Babinet scaling in the initial round), and the solvent contribution was included using a van der Waals radius of 1.0. At this stage, difference densities for the analysis of pore hydration were calculated (see Fig. 6). After adding some more water molecules, imidazole (where indicated at site S1), and at a few locations, other buffer components (glycerol, acetate, and sulfate where clearly defined in the density), 30 final refinement cycles led to the final models and refinement statistics (Table 2).

RESULTS

Expression of the His-168 and His-318 Variants—To test the proposed critical roles of His-168 and His-318, we constructed

14 variants of *E. coli* AmtB, replacing the histidines by non-polar (aromatic or aliphatic) and polar residues including potentially charged ones. These *amtB* alleles were introduced into a plasmid-borne *glnKamtB* operon and expressed in the Δ *glnK* Δ *amtB* strain GT1000. Eight of the variants behaved like wild-type AmtB in being correctly targeted to the inner membrane, in running as a major trimetric species with an apparent molecular mass of about 90 kDa on SDS-PAGE (Fig. 1A), and in their expression level (Fig. 1C). Six of the polar mutants (H168D, H168T, H318E, H168K, and the double mutants H168E/H318E and H168T/H318T) were still correctly targeted and well expressed but were also present, to a variable extent, as dimeric or monomeric species on SDS-PAGE (Fig. 2A, and data not shown for H168T/H318T), rendering the quantitative evaluation of their expression level difficult and indicating that they might be less stable.

AmtB-dependent GlnK Sequestering of the Variants—In almost all bacteria and archaea, *amtB* is genetically linked to *glnK*, which encodes a signal transduction protein (26, 27). GlnK is a member of the P_{II} family: trimeric proteins that act as sensors of cellular nitrogen status (27). Tyr-51 of GlnK is covalently modified by uridylylation in cells that are subject to nitrogen starvation, and this process is reversed in nitrogen sufficiency (28). A rapid increase in extracellular ammonium causes deuridylylated GlnK to interact with AmtB, apparently to regulate the activity of the channel in response to the intracellular nitrogen status (21).

In a previous study, we showed that a highly conserved AmtB residue, Asp-160, was essential for activity, insofar as an D160A mutation completely inactivated AmtB but did not affect the level of protein (21). We also showed that D160A AmtB was impaired in sequestering GlnK following an ammonium shock, despite GlnK being deuridylylated normally (21). The structure of AmtB shows that Asp-160, which is on the periplasmic side, has a critical structural role (7), and we deduce that any significant structural perturbation in AmtB may impair its interaction with GlnK either through perturbing oligomerization or by affecting the structure on the cytoplasmic face. Consequently, this interaction can be taken as indicative of a preserved native-like trimeric structure, and we therefore assessed the His variants of AmtB for their ability to sequester GlnK. All except H168T showed normal GlnK-AmtB complex formation (Fig. 3) and a normal deuridylylation pattern (data not shown) of GlnK after an ammonium shock of 30 mM for 15 min, suggesting that with one exception, they maintain a native-like structure. Interestingly, even the variants that appear less stable on SDS-PAGE (Fig. 2A) were able to form a complex with GlnK. None of the

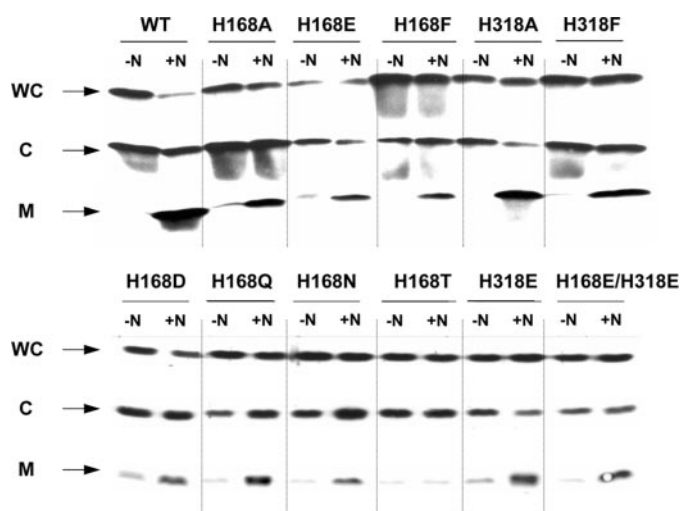


FIGURE 3. GlnK sequestration by AmtB assessed by Western blotting with anti-GlnK antibody. Each lane was loaded with 5 μ g of protein. Extracts were prepared from GT1000 (Δ *glnK* Δ *amtB*) expressing plasmid-encoded AmtB. Shown is a Western blot using an anti-GlnK antibody, after SDS-PAGE of whole-cell extracts (WC), cytoplasmic (C), and membrane (M) fractions before (–N) and after (+N) a 30 mM ammonium shock for 15 min. WT, wild type.

variant AmtB proteins was detected in the cytoplasmic fraction (Fig. 2A), indicating that they were all targeted to the membrane. Taken together, these results suggest that with the exception of H168T, the variants are all correctly folded and present as trimers in the membrane. The apparent destabilization of the trimeric state of some variants upon SDS treatment therefore does not imply that their structure is significantly perturbed under non-denaturing conditions.

X-ray Structure of Variants—Five of the functionally characterized His variants (H168A, H168E, H168F, H318A, H318F) and the H168A/H318A variant could be crystallized in the previously reported hexagonal form, which permitted their structure determination to a resolution of at least 2.2 Å resolution (8) (Table 2). When compared with wild-type AmtB, the structural changes were restricted to the mutated residue with minor changes in the conformation of the neighboring histidine in some cases (see Fig. 6, data not shown). Superposition of the 357 C α positions of the well ordered residues (Table 2) further illustrates this point. In the case of the H168F mutant, the His-318 side chain is rotated around χ 1 and χ 2 to avoid repulsive interactions. Even for the double mutant H168A/H318A, neither a structural collapse nor conformational adaptations in neighboring side chains are seen, indicating that the pore structure is intrinsically very rigid. The glutamate at position 168, which could be present in its protonated or charged form, appears as a very good mimic of the substituted imidazole. It occupies almost the same space, and its carboxylate is coplanar with the imidazole of His-318 and makes a hydrogen bond to its δ 1 nitrogen. In its protonated state, it also could act as hydrogen bond acceptor or donor for water/ammonium in the pore, depending on the tautomeric state of the two side chains.

His-168 and His-318 Are Essential for Optimum Substrate Conductance—The remarkable conservation of the two pore histidines led to the hypothesis that they play a key role in allowing the substrate to cross the central part of the channel (4,

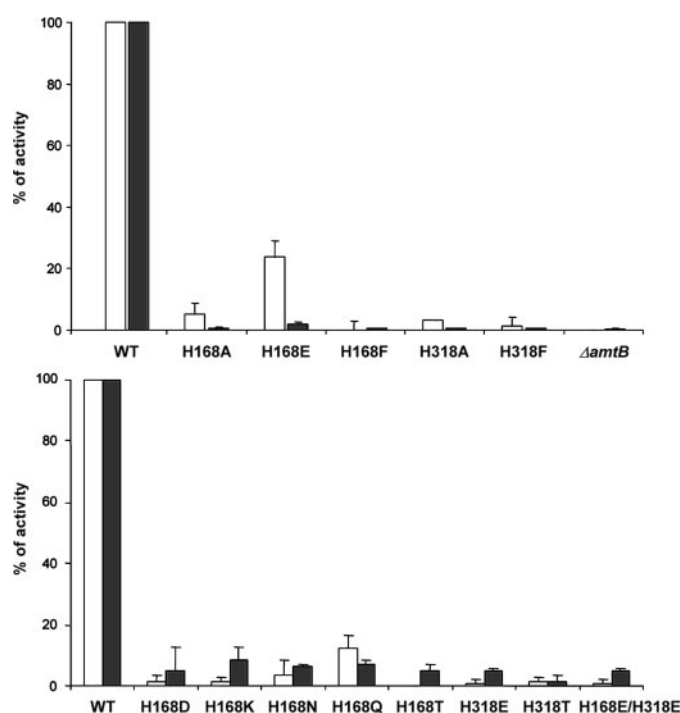


FIGURE 4. Activities of AmtB variants. White bars, [14 C]methylammonium accumulation (AmtB activity); gray bars, [14 C]methylglutamine accumulation (GS activity); results were measured by adding 20 μ M (final concentration) [14 C]methylammonium at time 0. Activities are a percentage of the activity in GT1000 (Δ *glnK* Δ *amtB*) expressing wild-type (WT) AmtB. For AmtB activity (white bars), the level in GT1000 (Δ *glnK* Δ *amtB*) has been subtracted.

7–9). Their precise function, whether to serve as proton acceptors for an entering ammonium ion, or more simply, to shape the pore and balance its polarity, has remained an open question, and no experimental data were available to confirm their proposed essential role.

We assessed the transport activities of each of the variants and detected no AmtB activity with any of them, except H168E, when using 20 μ M methylammonium as substrate (Fig. 4). As described in detail previously (10), in these assays, we measure both initial influx of methylammonium driven by the concentration gradient (AmtB activity) and its subsequent metabolic trapping by glutamine synthetase (GS activity). The H168E variant had a reduced but significant activity ($25 \pm 5\%$) when compared with wild type. No GS activity, in terms of conversion of methylammonium to methylglutamine, was detected in any case (Fig. 4) despite the level of GS protein and its distribution within the cell being equal to that of wild type in all strains (Figs. 1B and 2B). We have previously shown that GS activity is closely coupled to AmtB function (10), although the mechanism of this coupling is unknown. We hypothesize that the absence of GS activity, despite a low AmtB activity, for H168E is due to an incorrect metabolic linkage between the GS and AmtB. We therefore also measured GS activity in a H168E strain, using 1 and 2 mM external methylammonium. At 2 mM methylammonium, H168E had a GS activity of 54% when compared with the wild type, whereas a Δ *amtB* strain and the H168A variant showed a background activity of just 6% (Fig. 5). This confirms that H168E has significant activity.

To investigate the role of the conserved His residues further, we analyzed the location, height, and shape of residual

electron density peaks in and at the pore of AmtB for the wild type and all crystallized variant proteins. We hypothesized that this residual electron density might be a sensitive indicator of changes in the pore structure and of its surface and hydration properties. Such peaks have been interpreted as an ammonium binding site (Am1, at the periplasmic pore entry) (7, 8) and as partly occupied ammonia sites in the pore (designated Am2, Am3, and Am4) (7), or alternatively, as partly occupied water sites (8). We cannot experimentally discriminate between water and ammonium, and when talking about hydration and water binding sites below, it should be clear that both kinds of molecules could contribute to the observed difference density peaks. The fact that the observed difference density patterns were reproducible with data from different crystals of the same kind and robust against variation of the composition of the crystallization buffer (data not shown) and that they cannot arise from conformational disorder of the pore-lining side chains strongly indicate that

they indeed result from the distribution of water/ammonium molecules in the pore.

The inactive variants (H168A, H318A, H168F, H318F) show no density above 2σ at site S4, whereas the wild-type protein and the partly active H168E mutant show peaks above 4σ (Table 2 and Fig. 6). The best determined and probably fully occupied water molecules elsewhere in these structures show peak densities of up to 10σ in difference maps (data not shown). At a resolution of 2 Å, occupancies cannot be reliably determined, and using peak σ values will underestimate the occupancy of more mobile water molecules. The peak pattern at S3 is very similar to that at S4 with the exception of H168A, where a diffuse peak extending over sites S2 and S3 is observed. Apparently, the non-polar cavity generated at this site can trap some water that is not localized at defined positions. In the double mutant H168A/H318A, no significant peak is seen in the widened pore (Table 2) whose hydration appears to be below detectable levels. The non-polar mutants thus show reduced hydration and a loss of preferred water locations. The polar mutants have proven more difficult to handle, and sufficiently good crystals have only been obtained for the H168E variant, the only mutant that shows partial activity. We observe peaks between 5 and 6σ at S3 and S4 and a much larger peak at site S2, indicating the simultaneous presence of two water/ammonia molecules. Obviously, many arrangements appear possible, including the presence of a charged glutamate, perhaps even together with an ammonium ion-water pair. The presence of charged species would be expected to enhance pore hydration and could explain the increased height of all peaks when compared with the wild-type protein. An additional peak between site S3 and S4, present at reduced height also in the native protein structures, indicates the possible formation of a file of hydrogen-bonded water/ammonia molecules in this central part of the pore.

A number of the crystals examined contained high concentrations of imidazole (about 150 mM) in the buffer (Table 2). In all these cases, the site 1 density peak is above 10σ and appears flattened, suggesting that imidazole can occupy this site (Fig. 6). An imidazole added to the model refines with atomic *B*-factors that match very well those of the neighboring protein side chains, indicating that the peak cannot be due to partly occupied ammonium or water binding sites. As ammonium is also present at about 200 mM in the mother liquor, a protonated imidazole appears to compete efficiently with ammonium under these conditions.

DISCUSSION

The Twin-His Structure Is Essential for Optimum Substrate Conductance—The x-ray structure of *E. coli* AmtB (7, 8) revealed the central

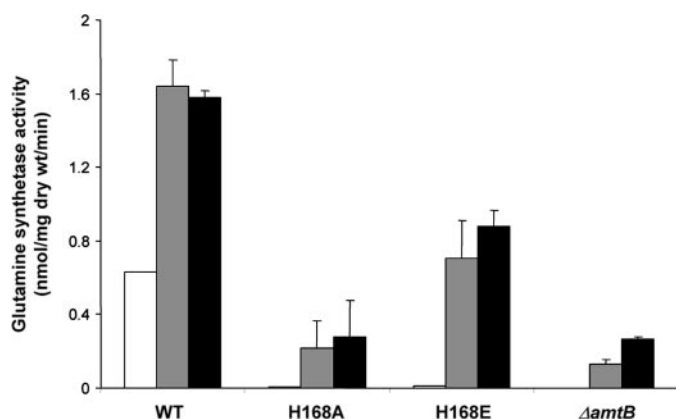


FIGURE 5. **GS activity.** [^{14}C]methylglutamine accumulation (GS activity) was measured after adding (final concentration) 20 μM (white bars), 1 mM (gray bars), 2 mM (black bars) of [^{14}C]methylammonium at time 0. Values are means \pm S.D. ($n = 6$). WT, wild type.

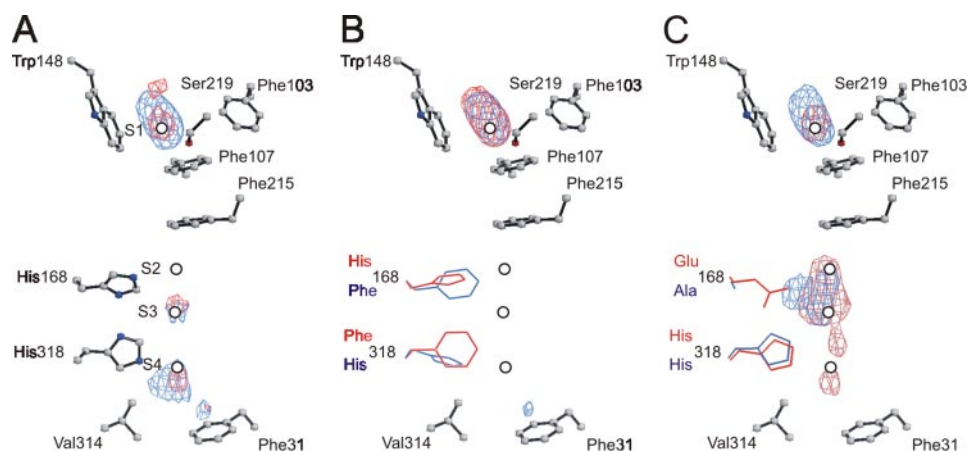


FIGURE 6. **Residual difference electron densities (contoured at 3σ) in the pore region.** Weighted difference density maps using (mFobs-DFcalc) terms as defined in Refmac (25) were used. Only the density peaks within a generous box ($7 \times 10 \times 22$ Å) covering the central pore region are displayed. Selected side chains at the periplasmic pore entry and along the pore are shown as ball-and-stick models. Positions corresponding to sites Am1-Am4 (7) are shown in black (S1-S4). A, difference densities from two native crystals in blue and red (buffer containing imidazole). B, difference densities and the side chains of residues 168 and 318 for the H168F and H318F in blue and red, respectively. C, difference densities and the refined side chains of residues 168 and 318 for H168A and H168E in blue and red, respectively. Except for H168A, all mutant crystals contain imidazole. The S4 peak position observed here is always about 1 Å closer to the cytoplasmic side than the Am4 site.

1	GGLLASHGALDFAGGTVVHINAAIAGLVGAYLIGKRVGFG	-189
2	HGWLYNLPALDFAGGGPVHIASGWAALAYAMVLGKRRDHG	-198
3	SGWLYKLGVDYFAGSGPVHIASGFGALAWSMLGPRVADS	-220
4	EGWLYKLGSLDYAGGLCVHLTSGHGGLVYALILGKRNPDV	-215
5	NGWLVSLGALDFAGGGPVHENSFGAALAYSMLGKRRHDPV	-209
6	NGWSFILGGLDFAGGTPVHISSGTAALAIISIFLGKRRGYG	-211
7	KGWSFVHGSYDFAGGTLVHISSGTAALAIISIFLGKRRGTA	-212
8	KGWANVMGGLDFAGGTPVHISSGTAALAIISIFLGKRRGYG	-216
9	NGWLYKLGELDFAGGGPVHITSGTAGFAWSLYLGGRRRGY	-210
10	SGWVFLGGLDFAGGTPVHIVSGTTALAYSMLGKRRGHG	-214
11	SGWVFNGLGGLDFAGGTPVHIASGSAALAYSMLGKRRGHG	-214
12	SGWSFRMGGLDFAGGTPVHISSGSAALAYSMLGKRRGHG	-221
13	NGWSFKLGGLDFAGGTPVHISSGAAALAYSMLGKRRAGYD	-215
14	NGWSFRMGGLDFAGGTPVHISSGAAALAYSMLGKRRGYN	-218
15	AGWSFRMGGLDYAGGTPVHIASGAAALAYSMLGPRRGHG	-225
16	NGWLNKLGSDYFAGGSPVHISSGMAALAYSIVIGKRCDHG	-215
17	NGWLYTLGALDFAGGGPVHISSGFAALAYSMLGRRIVVD	-214
18	GLLGENLGVLDFAAGGTPVHVCSGATATAISYLSYPLFRS	-196
19	NGWAFNYGVLDFAGGGPVHICSGLSALAYSMLGRRQERM	-234
20	NGWAFKYGVLDYAGGGPVHIGSGMAALAYSMLGRRQERM	-235
21	NGWAFKYGVMDYAGGGPVHIGSGVSALAYSMLGRRNEKM	-219
22	NGWAFKYGVLDYAGGGPVHIGSGMSALAYSMLGRRNEKM	-220
23	HGWAFKYGVLDFAGGGPVHIGSGVGLLAYAVLGRNRE	-197
24	GGWAYQWGVLDWAGGGNIHILSAVSGFVYSWFLGKRNEKL	-202
25	GGWAYQWGVLDWAGGGNIHILSAVAGFVYSYFLGRRKENL	-201
26	WASSYRSGALDYAGGGPVHIGSGMSAFVYSYFLGRRNETL	-211
27	NGWAFKFGVYDFAGGGPVHIGSGFAALAYTVCLGRRSKFV	-230
28	TGWAFKGVLDYAGGGPVHINSGITGLVISYLLGPRTYG	-230

FIGURE 7. **Alignment of the amino acid sequence of *E. coli* AmtB with fungal Amt sequences.** The sequence shown is the region around transmembrane helix M5, defined from the x-ray crystal structure of *E. coli* AmtB, for which the M5 residues are bounded by vertical lines. The conserved His-318 and the equivalent His/Glu residues are indicated in **bold**. The number of the last amino acid of the alignment for each sequence is indicated on the right. The number on the left indicates the origin of the sequence as follows: 1, *E. coli* AmtB; 2, *Aspergillus fumigatus* Amt1; 3, *Neurospora crassa* Amt4; 4, *Saccharomyces cerevisiae* Mep2; 5, *Candida albicans* Amt2; 6, *Hebeloma cylindrosporium* Amt1; 7, *H. cylindrosporium* Amt2; 8, *Ustilago maydis* Ump2; 9, *Mycrobotryum violaceum*; 10, *Aspergillus nidulans* MepA; 11, *A. fumigatus* Amt2; 12, *Tuber borchii* Amt1; 13, *Magnaporthe grisea* Amt3; 14, *N. crassa* MepA; 15, *M. grisea* Amt2; 16, *Saccharomyces pombe* Amt1; 17, *S. pombe* Amt2; 18, *N. crassa* Amt2; 19, *A. nidulans* MepA; 20, *A. fumigatus* MepA; 21, *N. crassa* Mep3; 22, *M. grisea* Amt1; 23, *H. cylindrosporium* Amt3; 24, *S. cerevisiae* Mep1; 25, *S. cerevisiae* Mep3; 26, *C. albicans* Amt2; 27, *S. pombe* Amt3; 28, *U. maydis* Mep1.

position of two conserved histidine side chains in the pore and suggested that they play a critical role in substrate conductance. In this mutagenesis study, we present the first experimental tests of this prediction and confirm their essential function for the conductance of the substrate analogue methylammonium and thus predictably also for ammonium.

Fundamental to our ability to draw this conclusion is the fact that with one exception, the variants are expressed at the wild-type level and targeted to the *E. coli* inner membrane. Furthermore, they maintain a native-like trimer structure, as indirectly assessed *in vivo* by their unperturbed interaction with GlnK or directly by x-ray crystallography of some of the variants. From these results, we conclude that the observed alterations in AmtB activity are due to a direct local effect at the substitution site and not to a change in the overall pore or protein structure.

Except for the partially active H168E mutant, which we show to be a good mimic of a histidine in this position, none of the other 13 variants comprising polar and non-polar substitutions of different size were active. This suggests a very specific functional role for the two histidines for which two kinds of explanation appear possible. First, their $\epsilon 2$ nitrogens might serve as proton acceptors for entering ammonium ions that could then traverse the central part of the

channel as ammonia and become reprotonated on the other side. Alternatively, efficient substrate conductance might require such a narrow mainly hydrophobic pore with a few rather precisely oriented hydrogen bond acceptor or donor functions for weak, stabilizing interactions with water/ammonia that still permit rapid diffusion. The more non-polar character of the AmtB channel when compared with aquaporins might provide some specificity for ammonia against water as the former is known to be more soluble in organic solvents. Our studies cannot discriminate between these two possibilities.

Against a role in substrate deprotonation, it can be argued that it is not obvious how the proton would be efficiently transferred back from His-168 across the Phe-107 and Phe-215 side chains to the cytoplasmic vestibule (4). Based on molecular dynamics studies, such a mechanism has also been rejected in favor of deprotonation occurring at the periplasmic ammonium binding site (15). An alternative fate for the proton, namely its separate transport through the pore, would correspond to net ammonium and thus electrogenic transport, which is not in accordance with experimental studies (7, 10). The fact that although the H168E mutant is partially active, neither H168D nor H318E show activity, further illustrates that activity depends on a combination of specific spatial and chemical properties of the pore and that the two histidines are not functionally equivalent despite the structural quasi-symmetry. Our crystallographic analysis of difference density peaks in the pore, which we interpret as partly occupied water or ammonium sites, reveals that only the H168E mutant maintains a native-like pattern. The protonation state of the glutamate is unknown, but the apparent enhanced level of pore hydration could be indicative of a charged state. Clearly, the peak pattern is very sensitive to the precise side chain architecture in the pore. The apparent correlation with activity is noteworthy; however, it cannot be concluded that the presence or absence of such a pattern is indicative of an active or inactive channel. AmtB crystallized in a different form (8) and Amt-1 from *A. fulgidus* (9) do not show significant residual densities in the pore, indicating that other factors also influence apparent pore hydration. In both those structures, the pore is wider on the cytoplasmic side of His-318 because of a conformational change at the N terminus of transmembrane helix 10 (7). In a slightly wider or more dynamic pore, hydration waters would distribute over larger volumes, and their density peaks might drop to noise levels. Despite this, we are convinced that within the crystal form that we have analyzed in this study, the different patterns can be reliably interpreted in terms of specific changes in pore hydration.

Amt/Rh Proteins That Do Not Contain the Twin-His Motif—Using *E. coli* AmtB as a model, we have shown that the two conserved histidine residues that characterize many members of the Amt/Rh family are indeed required for a fully functional channel. We might therefore conclude that these two histidines are a prerequisite for ammonia conductance. So what of those members of the Amt/Rh family, namely certain fungal Amts and the Rh30 proteins, that do not contain the twin-His motif?

In some fungal Amt proteins, a Glu residue replaces the first conserved His (Fig. 7). We have shown that substitution of His-168 by Glu in *E. coli* AmtB does not perturb the structure and that the variant protein retains an activity of about 25% when compared

with wild type. As previously proposed (4), it would indeed appear that the Glu residue occupies about the same space and can potentially make similar hydrogen-bonding interactions as the equivalent His residue. It is of interest to note that all the fungal species for which data are available encode multiple Amt proteins, at least one of which retains the twin-His motif (Fig. 7). Whether those fungal Amt proteins containing the natural Glu substitution have gained a specific biochemical or physiological function during evolution remains unclear.

In animals, the Amt homologues are the Rh proteins that have been most extensively characterized in humans. The glycosylated Rh proteins (RhAG, RhBG, and RhCG in humans) contain both conserved His residues and have been shown by a variety of approaches to be capable of ammonium transport (29). By contrast, in the non-glycosylated Rh30 proteins, which include the human erythrocyte RhD and RhCE proteins (30), the twin-His motif is not conserved (14). The equivalent residues to AmtB His-168 and His-318 are replaced by Tyr and Phe, respectively, and although they could provide weak C–H hydrogen bond donors and a phenolic OH group for polar interactions with substrate molecules (7), their ring orientation cannot be fixed by a hydrogen bond between them as occurs between the His residues in AmtB (7, 8).

The exact role of RhD and RhCE is uncertain, and these proteins have not been expressed in heterologous expression systems (e.g. yeast or oocytes) in the presence or absence of RhAG (29). However, stopped-flow studies on erythrocyte ghosts from human variants with defects of the Rh complex show that, by itself, RhD has no significant effect on ammonium transport (11). Based on these observations and our results with *E. coli* AmtB, it seems likely that Rh30 proteins do not function as ammonium channels but could have acquired a new function during evolution (29, 30).

In summary, our data not only demonstrate the utility of *E. coli* AmtB as a model system for dissection of the biology of the Amt protein family but also experimentally demonstrate the essential role of the twin-His motif (or very occasionally, a Glu-His pair) for Amt protein activity.

Acknowledgments—We thank Anne Durand and Tim Fulford for helpful comments on the manuscript, Emmanuele Severi for construction of pJT6E, Jeremy Thornton for anti-GlnK antibody, Wally van Heeswijk for anti-GS antibody, and Dirk Kostrewa for help with crystallographic analysis. Crystallographic data were collected at the Swiss Light Source, Paul Scherrer Institut, Switzerland, and we gratefully acknowledge the excellent help from Ehmke Pohl and Takashi Tomizaki.

REFERENCES

1. von Wirén, N., and Merrick, M. (2004) *Trends Curr. Genet.* **9**, 95–120
2. Marini, A.-M., Matassi, G., Raynal, V., Andre, B., Cartron, J. P., and Cherif-Zahar, B. (2000) *Nat. Genet.* **26**, 341–344
3. Westhoff, C. M., Ferreri-Jacobia, M., Mak, D. O., and Foskett, J. K. (2002) *J. Biol. Chem.* **277**, 12499–12502
4. Winkler, F. K. (2006) *Pfluegers Arch. Eur. J. Physiol.* **451**, 701–707
5. Blakey, D., Leech, A., Thomas, G. H., Coutts, G., Findlay, K., and Merrick, M. (2002) *Biochem. J.* **364**, 527–535
6. Conroy, M. J., Jamieson, S. J., Blakey, D., Kaufmann, T., Engel, A., Fotiadis, D., Merrick, M., and Bullough, P. A. (2004) *EMBO Rep.* **5**, 1153–1158
7. Khademi, S., O'Connell, J., III, Remis, J., Robles-Colmenares, Y., Miercke, L. J., and Stroud, R. M. (2004) *Science* **305**, 1587–1594
8. Zheng, L., Kostrewa, D., Bernèche, S., Winkler, F. K., and Li, X.-D. (2004) *Proc. Natl. Acad. Sci. U. S. A.* **101**, 17090–17095
9. Andrade, S. L., Dickmanns, A., Ficner, R., and Einsle, O. (2005) *Proc. Natl. Acad. Sci. U. S. A.* **102**, 14994–14999
10. Javelle, A., Thomas, G., Marini, A. M., Kramer, R., and Merrick, M. (2005) *Biochem. J.* **390**, 215–222
11. Ripoche, P., Bertrand, O., Gane, P., Birkenmeier, C., Colin, Y., and Cartron, J.-P. (2004) *Proc. Natl. Acad. Sci. U. S. A.* **101**, 17222–17227
12. Zidi-Yahiaoui, N., Mouro-Chanteloup, I., D'Ambrosio, A. M., Lopez, C., Gane, P., Le Van, K. C., Cartron, J. P., Colin, Y., and Ripoche, P. (2005) *Biochem. J.* **391**, 33–40
13. Mayer, M., Schaaf, G., Mouro, I., Lopez, C., Colin, Y., Neumann, P., Cartron, J. P., and Ludwig, U. (2006) *J. Gen. Physiol.* **127**, 133–144
14. Conroy, M. J., Bullough, P. A., Merrick, M., and Avent, N. D. (2005) *Br. J. Haematol.* **131**, 543–551
15. Lin, Y., Cao, Z., and Mo, Y. (2006) *J. Am. Chem. Soc.* **128**, 10876–10884
16. Smith, D. G., Garcia-Pedrajas, M. D., Gold, S. E., and Perlin, M. H. (2003) *Mol. Microbiol.* **50**, 259–275
17. Biswas, K., and Morschhauser, J. (2005) *Mol. Microbiol.* **56**, 649–669
18. Marini, A.-M., Soussi-Boudekou, S., Vissers, S., and Andre, B. (1997) *Mol. Cell. Biol.* **17**, 4282–4293
19. Zheng, L., Baumann, U., and Reymond, J. L. (2004) *Nucleic Acids Res.* **32**, e115
20. Coutts, G., Thomas, G., Blakey, D., and Merrick, M. (2002) *EMBO J.* **21**, 536–545
21. Javelle, A., Severi, E., Thornton, J., and Merrick, M. (2004) *J. Biol. Chem.* **279**, 8530–8538
22. Miroux, B., and Walker, J. E. (1996) *J. Mol. Biol.* **260**, 289–298
23. Studier, F. W. (2005) *Protein Expression Purif.* **41**, 207–234
24. Kabsch, W. (1993) *J. Appl. Crystallogr.* **26**, 795–800
25. Collaborative Computational Project No. 4 (1994) *Acta Crystallogr. Sect. D Biol. Crystallogr.* **50**, 760–763
26. Thomas, G., Coutts, G., and Merrick, M. (2000) *Trends Genet.* **16**, 11–14
27. Arcondéguy, T., Jack, R., and Merrick, M. (2001) *Microbiol. Mol. Biol. Rev.* **65**, 80–105
28. Jiang, P., Peliska, J. A., and Ninfa, A. J. (1998) *Biochemistry* **37**, 12782–12794
29. Van Kim, C. L., Colin, Y., and Cartron, J. P. (2006) *Blood Rev.* **20**, 93–110
30. Huang, C. H., and Peng, J. (2005) *Proc. Natl. Acad. Sci. U. S. A.* **102**, 15512–15517